Solar Energy Materials & Solar Cells 144 (2016) 438–444

Contents lists available at ScienceDirect

Solar Energy Materials & Solar Cells

journal homepage: www.elsevier.com/locate/solmat

Wearable organic solar cells with high cyclic bending stability: Materials selection criteria

Timothy F. O'Connor, Aliaksandr V. Zaretski, Suchol Savagatrup, Adam D. Printz, Cameron D. Wilkes, Mare Ivana Diaz, Eric J. Sawyer, Darren J. Lipomi *

Department of NanoEngineering, University of California, San Diego, 9500 Gilman Drive, Mail Code 0448, La Jolla, CA 92093-0448, United States

ARTICLE INFO

Article history:
Received 14 August 2015
Received in revised form
23 September 2015
Accepted 25 September 2015

Keywords:
Organic solar cell
Flexible electronics
Flexible solar cell
Conjugated polymer
Epidermal electronics
Wearable electronics

ABSTRACT

Despite the intrinsic flexibility of organic electronic materials due to their thinness, a deliberate selection of materials on the basis of their mechanical—not just charge-transport—properties is required for applications with mechanically demanding form factors, such as those that exist in the field of wearable electronics. This paper describes a skin-wearable solar cell enabled by the deliberate selection or intentional plasticization of the components to enable an extreme level of stability under cyclic bending deformations. In particular, poly(3,4-ethylenedioxythiophene):poly(styrenesulfonate) (PEDOT:PSS) films plasticized with 10% fluorosurfactant are used for both the anode and cathode, with the cathode layer further modified with polyethyleneimine (PEI) to lower the work function. Use of poly(3-heptylthiophene) (P3HpT) instead of the far more common poly(3-hexylthiophene) (P3HT) as the electron donor permitted extreme deformation because of its increased mechanical compliance (owing to its low glass transition temperature). Cells fabricated on 13-μm polyimide tape and adhered to human skin show stable performance when compressively strained by approximately 75%. These compressive strains produce convex and concave buckles with minimum radii of curvature of ca. 100 μm. Finite-element modeling predicts that the films require the ability to withstand a range of strains of 10%, when both convex and concave bends are considered. These devices, enabled by the stretchable semiconductor P3HpT, withstand up to one thousand cycles of compression with less than 20% degradation in power conversion efficiency, whereas devices based on P3HT show greater degradation after only five cycles, and fail catastrophically by fifty cycles. The usefulness of the wearable solar cells is demonstrated by their abilities to power an LED and a digital watch.

1. Introduction

The surest strategy to promote organic solar cells (OSCs) from laboratory-scale demonstrations to use in the real world is to exploit the advantages possessed by organics that would be difficult or impossible to replicate in more-efficient competing technologies [1]. Such advantages include low cost and embodied energy [2], extreme thinness [3], tunable color [4], biodegradability [5], semitransparency [6], extreme flexibility [3], and stretchability [7]. These characteristics suggest that portable power for displays [8], mobile health monitoring devices, and mitigation of climate change triggered by burning of biomass in the developing world are—far from applications dismissible as "niche"—important problems for which organic solar cells may provide the ideal solutions [9]. While the community has produced impressive demonstrations in ultra lightweight organic solar cells that can tolerate small bending radii [3], stability under cyclic deformation—required for real-world applications—has been poor. This fragility is a consequence of the fact that typical systems of materials are optimized overwhelmingly on the basis of efficiency on rigid substrates, as opposed to on the basis of mechanical stability. In this communication, we show that a deliberate selection of materials optimized for their mechanical properties can enable a new type of skin-mountable solar cell that can be used to power wearable electronic devices; these solar cells exhibit unprecedented stability to cyclic bending deformation. We performed these experiments to understand and anticipate routes of mechanical and photochemical degradation for all-organic solar cells under realistic operating conditions.

Despite the attractiveness of organic semiconductors for flexible and stretchable applications [1], the mechanical properties of these materials are highly variable, and there is a strong competition between compliance and charge transport [10]. The perceived compliance of optoelectronic polymers comes not because

* Corresponding author.
E-mail address: dlipomi@ucsd.edu (D.J. Lipomi).

http://dx.doi.org/10.1016/j.solmat.2015.09.049
0927-0248/

of their polymeric character, but because of the extreme thinness possible for the active layers of devices (ca. $\leq$100 nm) [11]. Thus unconventional active materials (e.g., liquid metals) [12], processing conditions, and device layouts [13,14] are generally required to produce devices stable enough to withstand extreme or repeated deformation, as would be encountered in ultra-thin, portable, or wearable applications [15]. The first wearable OSCs—i.e., integrated with clothing—were reported by Krebs in 2006 [16]. While these devices were flexible, the substrates and encapsulants were relatively thick ($>$250 μm total thickness), and thus mechanical compliance was not maximized [16].

The first stretchable organic solar cell was reported by Lipomi et al. in 2011 [17]. In this device, an organic active layer was coated on a poly(dimethylsiloxane) (PDMS) substrate under uniaxial tension. Release of the tension produced buckles in the active layer that accommodated subsequent cycles of strain. However, because of the unencapsulated liquid top contact—eutectic gallium-indium, an expensive material necessary to conform to the topography of the buckles—the device was not wearable because it could not be inverted [17]. Later, Kaltenbrunner et al. demonstrated an OSC on an ultrathin (1.4 μm) polyester foil capable of accommodating bending radii $\geq$10 μm [3]. This device represents the state of the art in ultrathin organic cells, but it showed poor stability under repeated compression when the whole device was mounted to an elastic substrate—27% reduction in efficiency after only 22 cycles of 50% compression—and all devices were measured in a nitrogen-filled glovebox [3]. Our goal was to fabricate devices that retained at least 80% of their initial efficiency up to 1000 cycles of loading, on the skin, and in outdoor sunlight, by selecting materials optimized on the basis of mechanical stability.

Our laboratory and others [18–20] have elucidated many of the molecular and microstructural parameters that permit the coexistence of good electronic performance with extreme mechanical compliance [7,15]. The process and materials we used are illustrated in Fig. 1 (see Supporting information for experimental details). We designed the device to have the "inverted" geometry (cathode on the bottom) and used a thin (13 μm) polyimide (PI) tape as the substrate. While substrates as thin as 1.4 μm have been used before [3], these substrates are not available with an adhesive, and are mechanically more fragile than thicker ones. Crucially, we used the elastomeric conjugated polymer poly(3-heptylthiophene) (P3HpT) [21]—in place of the typical poly(3-hexylthiophene) (P3HT)—because P3HpT is the first poly(3-alkylthiophene) with increasing length of the alkyl side chain whose glass transition is substantially below room temperature [22]. This property renders P3HpT about an order of magnitude less stiff than P3HT, and substantially more ductile [21]. The relative compliance of P3HpT compared to P3HT is preserved even when mixed with the typical fullerene acceptor, [6, 6]-phenyl C_{61} butyric acid methyl ester (PCBM), which is an antiplasticizer for poly(3-alkylthiophenes) (P3ATs) [21]. (In fact, the stiffening qualities of [60]PCBM are reduced when contaminated by up to 10% [70]PCBM—termed "technical grade" by manufacturers; thus, incompletely separated blends of methanofullerenes are substantially more compliant than pure samples, though we used 99% grade in this study for the sake of reproducibility) [23]. We used the typical transparent conductive polymer poly(3,4-ethylene dioxythiophene):poly(styrene sulfonate) (PEDOT:PSS) as both the anode and cathode [24]. We added 10% w/w Zonyl fluorosurfactant to the PEDOT:PSS solution to permit wetting on the PI substrate and also to plasticize the films by a factor of 100 relative to the unmodified

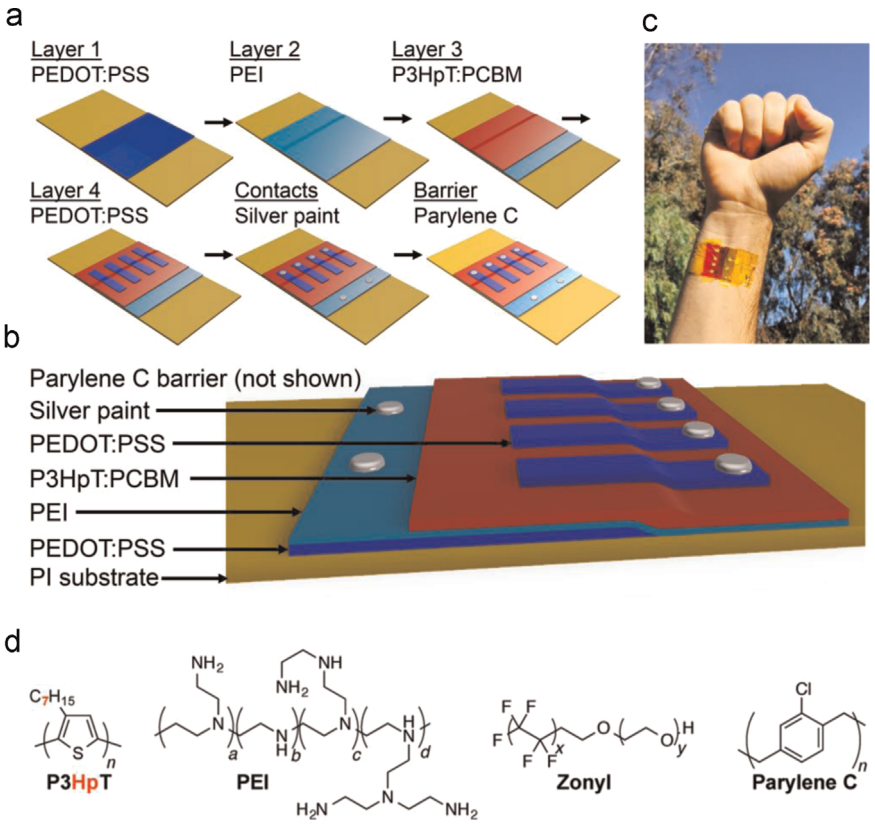

Fig. 1. Fabrication of ultra-flexible, wearable OSCs. (a) Schematic summary of the process used to fabricate wearable OSCs. Thin (13 μm) PI adhesive substrates were spin-coated with poly(3,4-ethylenedioxythiophene):poly(styrene sulfonate) (PEDOT:PSS), polyethyleneimine (PEI), and P3HpT:PCBM. PEDOT:PSS top-contacts are then transferred on top of the device using thermal release tape, and a strip of the active layer was wiped away to expose the bottom electrode. Silver paint was then applied to make electrical contact. (b) Schematic diagram of the cross section of a wearable OSC. (c) A photograph of the wearable solar cell on skin. (d) Chemical structures of the critical materials used in this study.

polymer [25]. The cathode layer was modified with poly(ethylene imine) (PEI) to lower the work function [24]. Casting this layer from ethanol instead of the usual methoxyethanol (MOE) produced a substantially more resilient film (crack onset strain 16.5% for ethanol and 3% for methoxyethanol) possibly because methoxyethanol is a better solvent than ethanol for the plasticizer, Zonyl, and washed it away during spin-coating. Table 1 is a summary of the crack-onset strains for conventional materials, and those modified for increased stability.

Optical micrographs of the devices prior to mechanical deformation indicate that the layers are undamaged (Fig. S1a). Electron microscopy revealed that the device is smooth at 5000× magnification (Fig. S1b). Devices were conformably adhered to the forearm of the experimenter, who provided written consent (Fig. 2a). (The only safety concern was the possibility of irritation from contact with the pressure-sensitive adhesive on the polyimide tape, which is sometimes produced by medical bandages, but which we did not observe.) We compressed the devices manually by approximately 75% (Fig. 2b). Fig. 2c shows an instance in which the strain was accommodated by a single concave buckle, which corresponds to a radius of curvature of 128 μm. We used finite element analysis (FEA) of the device on skin for both convex and concave buckles to calculate the strain in both tensile (Fig. 2d) and compressive modes. Simulations predicted peak strains of ± 5%. Since the active areas in the device could undergo either convex or concave buckling, we concluded that the active materials must be able to tolerate a dynamic range of strain of at least 10%.

Table 1
Summary of crack onset strains on polymeric supports for different materials. The most mechanically stable materials are indicated in bold. All materials were deposited or transferred onto poly(dimethylsiloxane) (PDMS) supports, except for aluminum and silver, which were evaporated directly on polyimide tape.

Component	Material	Crack-onset strain (%)	Reference
Cathode	Aluminum	< 1	This work
	Silver	< 1	This work
	PEDOT:PSS:(5%)Zonyl/ PEI(MOE)	3	This work
	PEDOT:PSS(5%)Zony/ PEI(EtOH)	**16.5 ± 2**	This work
Active layer (effect of polymer)	P3HT:[60]PCBM (99%)	1	This work
	P3HpT:[60]PCBM (99%)	**4 ± 1**	18
Active layer (effect of fullerene)	P3HT:[60]PCBM (99%)	1.25 ± 0.5	20
	P3HT:[60]PCBM:[70] PCBM (9:1)	1.75 ± 0.5	20
	P3HT:[60]PCBM:[70] PCBM (1:1)	**5.0 ± 1.0**	20
Anode	PEDOT:PSS	5 ± 1	22
	PEDOT:PSS:(10%) Zonyl	**35 ± 2**	22

The yield of functional cells was 41 of 44 (93%). One cell from each substrate was selected to measure the stability of the photovoltaic properties when strained. Fig. 3a shows a representative plot of the evolution of current density vs. voltage (*J*–*V*) for a cell as it was subjected to 1000 cycles of 75% global compressive strain. Because these unencapsulated devices were measured in ambient air, the total degradation represents a superposition of the chemical degradation [26] and the mechanical degradation [15]. Fig. 3b illustrates this point by plotting the average normalized *PCE* of five cells that underwent mechanical deformation as a function of the number of cycles, and of five cells that were uncycled. For the uncycled samples, the data points correspond to the time (upper *x*-axis) taken to apply strain to the cycled device. On average, devices subjected to 1000 strain cycles retained 81.5 ± 1.9% of their initial efficiency, while uncycled cells retained 88.4 ± 1.4% (Fig. 3b). Strained cells exhibited a sharp decrease in performance over the first 100 cycles. Devices exhibited similar behavior when measured in outdoor sunlight (Fig. 3c). For comparison, seven substrates bearing four devices each were fabricated using P3HT:PCBM—as opposed to P3HpT:PCBM—as the active layer; five devices exhibited catastrophic failure before 400 cycles, and two failed as early as 25 cycles (one of which is represented in Fig. 3d). Devices were worn for less than 15 min at a time, and the chemical barrier properties of PI are sufficient to prevent exposure to the organic electronic materials or surfactants.

In order to understand the origin of the reduction in performance, we characterized the cells before and after mechanical cycling using optical microscopy. The optical micrographs depicted in Fig. S2 exhibit little sign of mechanical deterioration in the cells before mechanical cycling (Fig. S2a), whereas devices that had been subjected to 1000 strain cycles (Fig. S2b) showed signs of damage in the form of pinhole fractures and microscopic, localized delamination (Fig. S2c). To isolate the possible effects of damage to the PEDOT:PSS electrodes, we measured the electrical conductivity of these films (PEDOT:PSS on PI) under the same conditions of

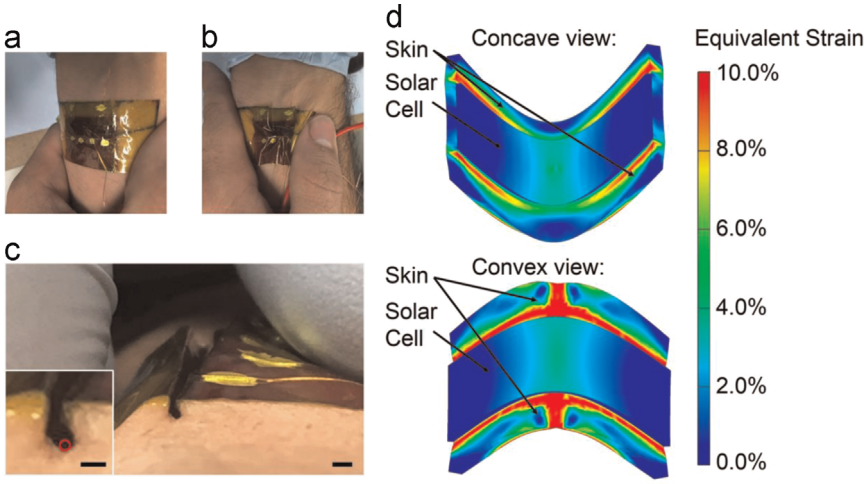

Fig. 2. Mechanical deformation of OSCs on skin. (a) Photograph of a wearable OSC under compression. (b) Magnified image of the compression buckle on the solar cell device for clarity (scale bar = 500 μm). (c) Fitted circles of radius 128 μm for an estimate of the radius of curvature (scale bar = 500 μm). (d) Finite element analysis of PI substrates deformed with corresponding radius of curvature.

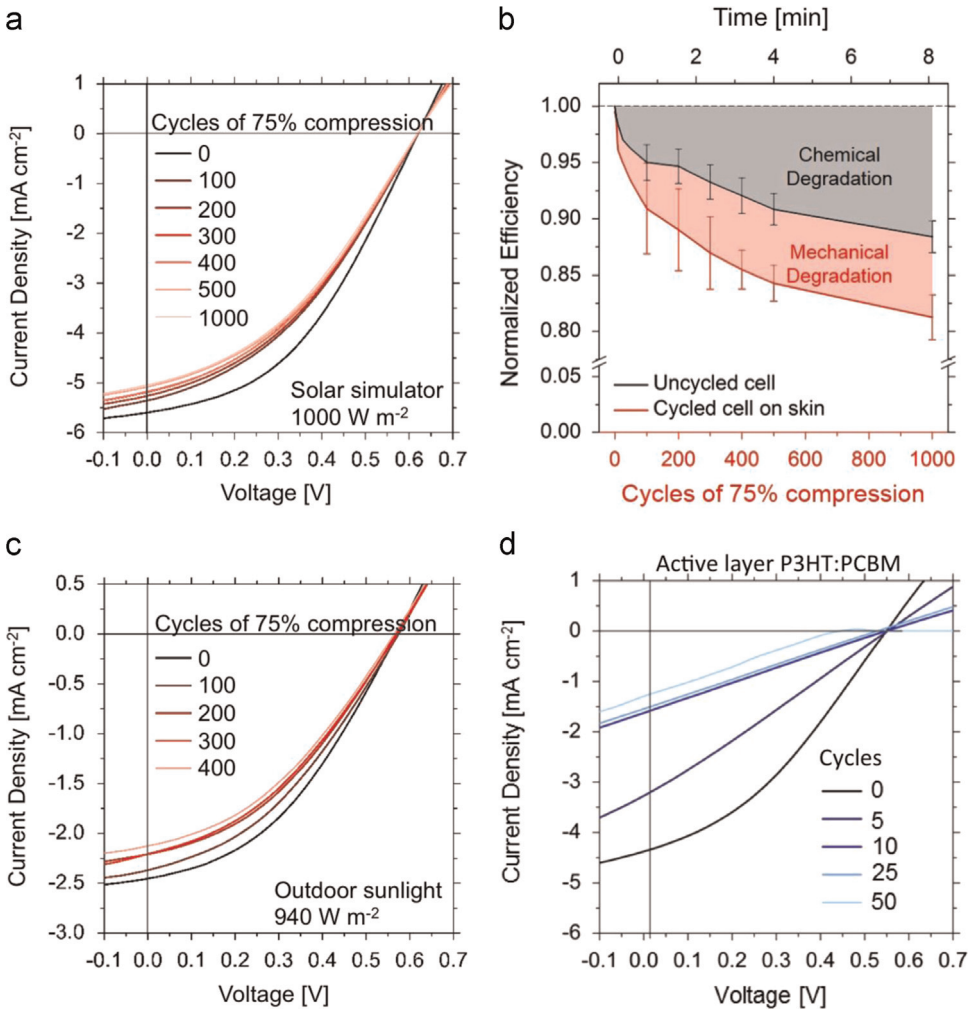

Fig. 3. Electrical characteristics of wearable solar cells with mechanical deformation and in the outdoor environment. (a) Electronic characterization of the devices measured in air over 1000 cycles of 75% compression. (b) Normalized efficiency of wearable solar cells over 1000 cycles at 75% strain (red) and of undeformed control cells whose properties were measured at time points that corresponded to the time required to compress the sample (black). (c) Degradation over 400 cycles for a wearable solar cell measured in outdoor sunlight. (d) Representative plot of the evolution in photovoltaic properties of a wearable solar cell whose active layer comprised P3HT:PCBM (not P3HpT:PCBM) from 0 to 50 cycles of 75% compression. (For interpretation of the references to color in this figure legend, the reader is referred to the web version of this article.)

cyclic compression as used for the complete cells. We observed no change in resistance over 1000 cycles of 75% compression.

To increase the stability of the devices against photochemical degradation for outdoor applications, a 1-μm barrier of parylene C was vapor deposited on the devices before attaching them to the skin. The practicality of these devices was then demonstrated by powering three different electronic devices (Fig. 4a–c). The images in Fig. 4a and b show wearable OSCs on skin powering a digital watch and an LED under 980 W m^{-2} of natural sunlight, as determined using a Daystar DS-05 A digital solar meter. Fig. 4c shows the charging of a portable battery (though this device was powered by the solar simulator in the glovebox, see below). The *I–V* characteristics of these devices are plotted in Fig. 4d and e. Many low power devices, such as digital watches or biosensors, require only modest currents to function, but larger voltages than are generated by single-cell OSCs (e.g., 1.8 V and ~100 μA in the case of the digital watch). In order to produce the voltages required to power the watch, OSCs on a single substrate were wired in series to produce a device with a V_{OC} of 2.23 V, and an operational voltage of V_{watch}=2.18 when measured in the glovebox. The LED circuit required a minimum of 0.4 V and ~1 mA, which were achieved using two substrates and 8 cells. To activate the charging mode on the portable battery, 15 cells were wired in series yielding a device with a V_{pp} of 4.66 V and a $I_{max\ power}$ of 201 μA. Because of the delicate nature of this device (i.e., number of wires needed to achieve V_{OC}~8 V), it was not removed from the glovebox.

We then analyzed the effect of the 1-μm barrier of parylene C on the degradation of the devices on planar substrates (Fig. 4f). During the first 10 min (taken to prepare devices for measurement outside the glovebox), we measured an average loss in efficiency of 36.4 ± 1.0% in the devices with no barrier, while protected devices only suffered a decrease of 4.8 ± 2.1%. The degradation was monitored every hour over the course of 5 h, after which the unencapsulated devices retained only 42.5 ± 3.3% of their initial efficiency, while encapsulated cells retained 82.3 ± 3.4%. Contrary to our expectations, the encapsulant did not increase the mechanical stability of these devices despite shifting the active materials closer to the neutral plane [27]. After 1000 cycles of compression, encapsulated devices retained 68% of their initial efficiency. From this pilot experiment (three devices), the mechanical stability of devices that were encapsulated with 1 μm or 10 μm of parylene C was worse than any device without a barrier. Further, unlike the unencapsulated devices, whose mechanical degradation was insignificant between 500 and 1000 cycles of compression (Fig. 3a), encapsulated devices continued to degrade mechanically

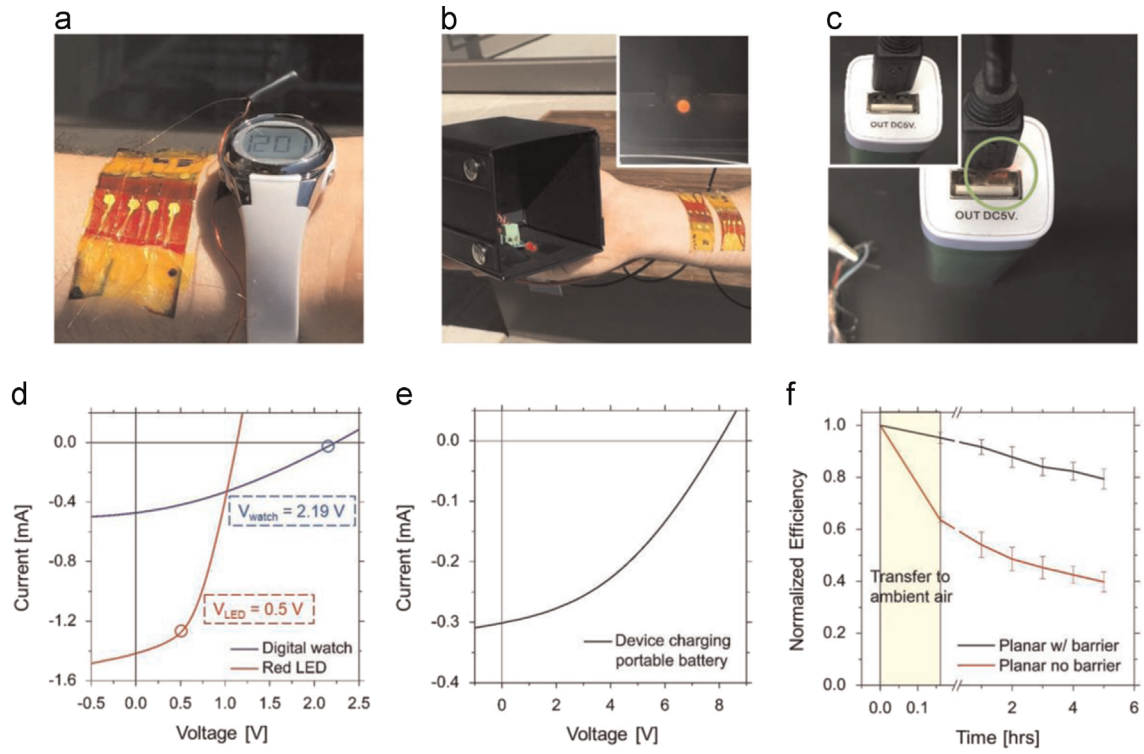

Fig. 4. Applications of wearable OSCs. Wearable OSCs on skin powering: (a) a wearable digital watch in outdoor sunlight and (b) an LED in a minimalist Armstrong self-oscillating voltage booster circuit (a.k.a. a joule thief circuit) in outdoor sunlight (980 W m^{-2}). (c) Wearable OSCs on a flat substrate powering a portable battery under 1 Sun illumination of a solar simulator (the green circle shows that the battery pack is in charging mode and the inset clarifies that the device is not charging when there is no incident light on the OSC). Devices remained in the glove box and were illuminated by a solar simulator. (d) Current-voltage characteristics of P3HpT:PCBM OSCs powering an LED (red), digital watch (blue) and (e) charging a portable battery. Measurements were taken in the glove box with illumination provided by a solar simulator. (f) Degradation characteristics of bare and parylene C encapulated OSCs in the laboratory air on planar substrates. The shaded area represents the degradation due to transferring the devices from within the glove box to their first measurement $t=0$. (For interpretation of the references to color in this figure legend, the reader is referred to the web version of this article.)

throughout the experiment. We attribute the increased mechanical degradation of the encapsulated devices to residual interfacial stress between the PEDOT:PSS top contact and the vapor-deposited parylene C film.

In summary, this work described the first organic solar cell conformally bonded to human skin. This device was enabled by the deliberate selection of semiconductors and electrodes that are known to exhibit intrinsic mechanical compliance—as opposed to compliance based on microfabricated relief structures [28] or fractal designs [29,30]. While this research used the organic solar cell as a model device, the knowledge generated of the materials, mechanics, and processing should be easily transferred to wearable and textile based organic light-emitters, RFID tags, thermoelectrics, and field-effect transistors for the burgeoning field of wearable electronics, mobile health monitors, electronic skin, and roll-to-roll processed organic devices exhibiting extreme mechanical stability.

2. Methods

2.1. Materials

Poly(3-hexylthiophene) (P3HT, M_n=44 kDa, PDI=2.0) and poly (3-heptylthiophene) (P3HpT, M_n=35 kDa, PDI=1.5) were produced by Rieke Metals, Inc. (P3HpT was obtained directly from Rieke Metals, Inc.; P3HT was produced by Rieke Metals, Inc., but sold by Sigma-Aldrich.) PDMS, Sylgard 184 (Dow Corning), was prepared according to the manufacturer's instructions at a ratio of 10:1 (base:crosslinker) and cured at room temperature for 36 to 48 h before it was used for mechanical testing. (Tridecafluoro-1,1,2,2-tetrahydrooctyl)-1-trichlorosilane (FOTS) was obtained from Gelest. PEDOT:PSS (Clevios PH1000) was purchased from Heraeus. DMSO was purchased from BDH with purity of 99.9% and Zonyl (FS-300) fluorosurfactant were purchased from Sigma-Aldrich. Chloroform ($CHCl_3$), ortho-dichlorobenzene (ODCB), acetone, isopropyl alcohol (IPA), and ITO-coated glass slides were obtained from Sigma-Aldrich and used as received. Zonyl (FS-300) fluorosurfactant, PEI, chloroform, ODCB, and isopropanol were purchased from Alfa Aesar. The PI tape was obtained from Caplinq, product number PIT0.5S UT/25.4. Leitsilber conductive silver paste was obtained from Ted Pella Inc. Thermal release tape (Revalpa 3196) was obtained from Nitto Denko.

2.2. Fabrication of epidermal OSCs

A step-by-step summary of the process used to fabricate the epidermal OSCs is shown in Fig. 1a. The total thickness of the device was 13.7 μm, which comprised a 13-μm-thick PI substrate bearing a pressure-sensitive adhesive, a 190 nm PEDOT:PSS bottom-contact with a 10 nm PEI surface treatment to lower its work function (cathode) [20], a 130 nm P3HpT active layer, and a 250 nm PEDOT:PSS top-contact (anode). The substrate was prepared by adhering a 1 × 2-in strip of 13 μm PI tape to a glass slide, upon which the bottom electrode was deposited by spin coating a solution of PEDOT:PSS/DMSO/Zonyl (84:6:10) for 240 s at 400 rpm. The bottom contact was then heated for 30 min at 120 °C. Scotch tape was then used to pattern the bottom contact (by stripping unwanted regions) into a 1 × 0.75-in rectangle, such that the 1-in side occupied the entire width of the tape. Subsequently, the work function of the bottom electrode was lowered by depositing a surface layer of PEI by spin coating a 1.5% w/w solution of PEI in

EtOH. The PEI was spin-coated in a 1×1-in region, as it also promoted the adhesion between P3HpT:PCBM and the PI tape in the subsequent step. The PEI layer was then heated at 110 °C for 10 min. The active layer was then added by spin-coating a 40 mg mL^{-1} solution of P3HpT:PCBM (1:1) in ODCB for 240 s at 500 rpm, then 15 s at 2 krpm. The device was then heated at 110 °C for 22 min in inert atmosphere. The top contacts were transferred to the device using thermal release tape. PEDOT:PSS/DMSO/Zonyl was spin coated on the adhesive side of the thermal release tape for 240 s at 400 rpm. The tape was then cut into strips of the desired contact size and adhered to the surface of the device such that the PEDOT/PSS/Zonyl layer was in direct interface with the P3HpT:PCBM layer. The transfer was completed in an inert atmosphere by placing the devices on a hotplate that had been pre-heated to 135 °C for 30 s. It is critical to note that the top contact was positioned in an offset fashion from the bottom contact, such that a portion of the top contact did not have the bottom contact below it (see Fig. 1b). If the silver paint was applied to the top-contact while the bottom contact was directly below, the silver paint shorted the top and bottom electrodes. The devices were then transferred from their glass substrates to wax paper substrates. The low energy surface of the wax paper reduced the adhesion of the substrate to its platform, and significantly decreased the incidence of delamination of the silver contact during transfer from the substrate used for fabrication to the skin. Lastly, silver paint and copper wires were added to the top contacts to make electrical contact with measurement equipment. Small strips of PI tape were used to secure the silver contacts during transfer and compression.

2.3. Yield

Of the forty-four devices prepared during the course of this study, three were not operational. Two of these devices exhibited short circuits and one exhibited an open circuit due to failure of a top contact to transfer. The average initial power conversion efficiency (*PCE*) for substrate-mounted devices in the glovebox was 1.02%, with a range from 0.7% to 1.71%. The initial average *PCE* of skin-mounted devices (before mechanical testing) was 1.16% with a range of 0.79–1.39% and the average final efficiency (1000 cycles of 75% compression) was measured to be 0.96% with a range of 0.6–1.19%. The reported average PCE for the skin-mounted cells is higher than the average for substrate-mounted cells because the skin-mounted cells (the best cell on each of five substrate bearing four cells each) were the best-performing subset of all devices made (all working cells on all substrates). As the goal of this study was to demonstrate a new purpose for ultra-flexible OSCs, we did not try to optimize the efficiency. The use of PEDOT:PSS as both the top and bottom contacts—and in particular, the lack of a reflective electrode, which ordinarily permits light to pass through the active layer a second time—and the roughness of the PI tape (Fig. S2a) could partially explain the initial efficiency that is less than that reported by other groups for ultrathin substrates [3]. The films were not observed to be rough on the nanoscale (Fig. S2b).

2.4. Mechanical simulations

In order to obtain the strain distribution maps of the cells under compression cycles, a computer-assisted design (CAD) model of a skin patch with the polyimide tape attached to it was created in Autodesk Inventor 2015 suite with the corresponding material parameters applied to both parts. The modeled PI tape dimensions were 13 by 400 by 1200 μm^3, the skin patch dimensions were 52 by 800 by 1200 μm^3. A static linear finite element analysis (FEA) simulation of the buckling of the cells was then performed by bending the skin-supported PI tape around a rigid cylinder of the appropriate radius that corresponded to the typical experimentally measured bending radius of the cells, i.e., 128 μm. For the simulation, the skin/PI interface was selected as "bonded," while the skin/cylinder interface was selected as "sliding/no separation" in order to avoid extraneous stress on the assembly. The mesh size was selected as the 0.05 fraction of the smallest dimension of a part, while the minimal element size was the 0.1 fraction of the mesh size. The constraints were the following: the cylinder was fixed with zero degrees of freedom and the assembly was symmetrically aligned to the axis of the cylinder while maintaining the tangential constraint between the cylinder surface and the skin surface (in the case of concave bending) and the PI film surface (in the case of convex bending). Further a 0.1 N force was applied to the PI film edges parallel to the cylinder axis in order to induce bending. Maps of equivalent strain were obtained and the color bar scale was constrained to represent maximum 10% strain in order to not oversaturate the strain map on the PI surface (skin has a much lower elastic modulus and strains to a much higher degree). We note that the deformation of the skin in the vicinity of the device is substantial because of the mismatch in mechanical properties between the PI tape (tensile modulus = 2.5 GPa) and the skin (0.02 GPa).

2.5. Cycling studies

Wearable OSCs were transferred from their fabrication platforms to the skin, then cycled at 75% strain in ambient conditions (i.e., outside of the glovebox) for up to 1000 cycles. The strain cycling was performed by manually compressing the device by 75%. Image analysis was used to measure the amount of compression. OSCs were also subjected to cycling outdoors, under natural sunlight.

2.6. Crack-onset measurements

To measure crack on-set strain, the polymer films were prepared by spin-coating to produce a film of ~100 nm thickness. The films were then transferred onto unstrained PDMS rectangles. The rectangles were then stretched from 0% to the crack-onset strain using a linear actuator with a step size of 0.5% using a computer-controlled stage. At each step, optical microscope images of the films were taken in order to observe the generation of cracks. The crack on-set strain of each conjugated polymer was defined as the strain at which the first crack was observed. To determine the crack-onset of metal films, the metals were deposited onto PI substrates though thermal evaporation, and subsequently strained on the PI substrates, without transfer to PDMS.

2.7. Barrier studies

A parylene C barrier of 1 μm thickness was deposited on wearable OSCs by means of vapor deposition using a PDS 2010 Parylene Coater. OSCs were transported to the parylene coater in inert atmosphere, limiting the effect of chemical degradation to roughly 30 s. After encapsulation, devices were protected from light as they were transported back to inert atmosphere for measurement and storage. Encapsulated and unencapsulated solar cells were subject to ambient conditions (i.e., atmospheric environment and 0.03 W m^{-2} of light) between measurements and were only exposed to intense (1000 W m^{-2}) illumination during measurement.

2.8. Powering devices

The digital watch was powered by a four solar cells on a single substrate. The cells were separated using a razor blade, then wired

together in series. The LED circuit was powered using two substrates. The four cells on each substrate were first wired together in parallel, creating a two devices each with four times the effective area. These two devices were then wired in series. The portable battery was powered by wiring 15 cells in series. All of the individual cells had areas of approximately 0.1 cm^2.

Acknowledgments

This work was supported by the Air Force Office of Scientific Research (AFOSR) Young Investigator Program, Grant number FA9550-13-1-0156. T.O. acknowledges support from the National Defense Science and Engineering Graduate Fellowship. S.S. and A. Z. acknowledge support provided by the National Science Foundation Graduate Research Fellowship.

Appendix A. Supplementary material

Supplementary data associated with this article can be found in the online version at http://dx.doi.org/10.1016/j.solmat.2015.09.049.

References

[1] L.T. Dou, J.B. You, Z.R. Hong, Z. Xu, G. Li, R.A. Street, Y. Yang, 25th Anniversary article: a decade of organic/polymeric photovoltaic research, Adv. Mater. 25 (2013) 6642–6671.
[2] N. Espinosa, M. Hosel, D. Angmo, F.C. Krebs, Solar cells with one-day energy payback for the factories of the future, Energy Environ. Sci. 5 (2012) 5117–5132.
[3] M. Kaltenbrunner, M.S. White, E.D. Glowacki, T. Sekitani, T. Someya, N. S. Sariciftci, S. Bauer, Ultrathin and lightweight organic solar cells with high flexibility, Nat. Commun. 3 (2012) 770.
[4] C.M. Amb, M.R. Craig, U. Koldemir, J. Subbiah, K.R. Choudhyry, S.A. Gevorgyan, M. Jorgensen, F.C. Krebs, F. So, J.R. Reynolds, Aesthetically pleasing conjugated polymer:fullerene blends for blue-green solar cells via roll-to-roll processing, ACS Appl. Mater. Interfaces 4 (2012) 1847–1853.
[5] M. Strange, D. Plackett, M. Kaasgaard, F.C. Krebs, Biodegradable polymer solar cells, Sol. Energy Mater. Sol. Cells 92 (2008) 805–813.
[6] J.Y. Lee, S.T. Connor, Y. Cui, P. Peumans, Semitransparent organic photovoltaic cells with laminated top electrode, Nano Lett. 10 (2010) 1276.
[7] S. Savagatrup, A.D. Printz, T.F. O'Connor, A.V. Zaretski, D.J. Lipomi, Molecularly stretchable electronics, Chem. Mater. 26 (2014) 3028–3041.
[8] M.S. White, M. Kaltenbrunner, E.D. Glowacki, K. Gutnichenko, G. Kettlgruber, I. Graz, S. Aazou, C. Ulbricht, D.A.M. Egbe, M.C. Miron, Z. Major, M. Scharber, T. Sekitani, T. Someya, S. Bauer, N.S. Sariciftci, Ultrathin, highly flexible and stretchable PLEDs, Nat. Photonics 7 (2013) 811–816.
[9] F.C. Krebs, T.D. Nielsen, J. Fyenbo, M. Wadstrom, M.S. Pedersen, Manufacture, integration and demonstration of polymer solar cells in a lamp for the "Lighting Africa'' initiative, Energy Environ. Sci. 3 (2010) 512–525.
[10] O. Awartani, B. Lemanski, H.W. Ro, L.J. Richter, D.M. DeLongchamp, B.T. O'Connor, Correlating stiffness, ductility, and morphology of polymer: fullerene films for solar cell applications, Adv. Energy Mater. 3 (2013) 399–406.
[11] J.A. Rogers, M.G. Lagally, R.G. Nuzzo, Synthesis, assembly and applications of semiconductor nanomembranes, Nature 477 (2011) 45–53.
[12] J.H. So, H.J. Koo, M.D. Dickey, O.D. Velev, Ionic current rectification in soft-matter diodes with liquid-metal electrodes, Adv. Funct. Mater. 22 (2012) 625–631.
[13] M. Kaltenbrunner, T. Sekitani, J. Reeder, T. Yokota, K. Kuribara, T. Tokuhara, M. Drack, R. Schwodiauer, I. Graz, S. Bauer-Gogonea, S. Bauer, T. Someya, An ultra-lightweight design for imperceptible plastic electronics, Nature 499 (2013) 458–463.
[14] H.S. Wu, S. Kustra, E.M. Gates, C.J. Bettinger, Topographic substrates as strain relief features in stretchable organic thin film transistors, Org. Electron. 14 (2013) 1636–1642.
[15] S. Savagatrup, A.D. Printz, T.F. O'Connor, A.V. Zaretski, D. Rodriquez, E.J. Sawyer, K.M. Rajan, R.I. Acosta, S.E. Root, D.J. Lipomi, Mechanical degradation and stability of organic solar cells: molecular and microstructural determinants, Energy Environ. Sci. 8 (2015) 55–80.
[16] F.C. Krebs, M. Biancardo, B. Winther-Jensen, H. Spanggard, J. Alstrup, , Strategies for incorporation of polymer photovoltaics into garments and textiles, Sol. Energy Mater. Sol. Cells 90 (2006) 1058–1067.
[17] D.J. Lipomi, B.C.-K. Tee, M. Vosgueritchian, Z.N. Bao, Stretchable organic solar cells, Adv. Mater. 23 (2011) 1771–1775.
[18] J. Liang, L. Li, K. Tong, Z. Ren, W. Hu, X.F. Niu, Y.S. Chen, Q.B. Pei, Silver nanowire percolation network soldered with graphene oxide at room temperature and its application for fully stretchable polymer light-emitting diodes, ACS Nano 8 (2014) 1590–1600.
[19] J.J. Liang, L. Li, X.F. Niu, Z.B. Yu, Q.B. Pei, Elastomeric polymer light-emitting devices and displays, Nat. Photonics 7 (2013) 817–824.
[20] Z.B. Yu, X.F. Niu, Z. Liu, Q.B. Pei, Intrinsically stretchable polymer light-emitting devices using carbon nanotube-polymer composite electrodes, Adv. Mater. 23 (2011) 3989–3994.
[21] S. Savagatrup, A.D. Printz, H.S. Wu, K.M. Rajan, E.J. Sawyer, A.V. Zaretski, C.J. Bettinger, D.J. Lipomi, Viability of stretchable poly(3-heptylthiophene) (P3HpT) for organic solar cells and field-effect transistors, Synth. Met. 203 (2015) 208–214.
[22] S. Savagatrup, A.D. Printz, D. Rodriquez, D.J. Lipomi, Best of both worlds: Conjugated polymers exhibiting good photovoltaic performance and high tensile elasticity, Macromolecules 47 (2014) 1981–1992.
[23] S. Savagatrup, D. Rodriquez, A.D. Printz, A. Sieval, J.C. Hummelen, D.J. Lipomi, [70]PCBM and incompletely separated grades of methanofullerenes produce bulk heterojunctions with increased robustness for ultra-flexible and stretchable electronics, Chem. Mater. 27 (2015) 3902–3911.
[24] Y.H. Zhou, C. Fuentes-Hernandez, J.W. Shim, J. Meyer, A.J. Giordano, H. Li, P. Winget, T. Papadopoulos, H. Cheun, J. Kim, M. Fenoll, A. Dindar, W. Haske, E. Najafabadi, T.M. Khan, H. Sojoudi, S. Barlow, S. Graham, J.L. Bredas, S.R. Marder, A. Kahn, B. Kippelen, A universal method to produce low-work function electrodes for organic electronics, Science 336 (2012) 327–332.
[25] S. Savagatrup, E. Chan, S. Renteria-Garcia, A.D. Printz, A.V. Zaretski, T.F. O'Connor, D. Rodriquez, E. Valle, D.J. Lipomi, Plasticization of PEDOT:PSS by common additives for mechanically robust organic solar cells and wearable sensors, Adv. Funct. Mater. 25 (2015) 427–436.
[26] M. Jorgensen, K. Norrman, S.A. Gevorgyan, T. Tromholt, B. Andreasen, F.C. Krebs, Stability of polymer solar cells, Adv. Mater. 24 (2011) 580–612.
[27] D.H. Kim, J.A. Rogers, Stretchable electronics: materials strategies and devices, Adv. Mater. 20 (2008) 4887–4892.
[28] J. Lee, J.A. Wu, M.X. Shi, J. Yoon, S.I. Park, M. Li, Z.J. Liu, Y.G. Huang, J.A. Rogers, Stretchable GaAs photovoltaics with designs that enable high areal coverage, Adv. Mater. 23 (2011) 986–991.
[29] J.A. Fan, W.H. Yeo, Y.W. Su, Y. Hattori, W. Lee, S.Y. Jung, Y.H. Zhang, Z.J. Liu, H.Y. Cheng, L. Falgout, M. Bajema, T. Coleman, D. Gregoire, R.J. Larsen, Y. G. Huang, J.A. Rogers, Fractal design concepts for stretchable electronics, Nat. Commun. 5 (2014) 3266.
[30] D.H. Kim, N.S. Lu, R. Ma, Y.S. Kim, R.H. Kim, S.D. Wang, J. Wu, S.M. Won, H. Tao, A. Islam, K.J. Yu, T.I. Kim, R. Chowdhury, M. Ying, L.H. Xu, M. Li, H.J. Chung, H. Keum, M. McCormick, P. Liu, Y.W. Zhang, F.G. Omenetto, Y. Huang, T. Coleman, J.A. Rogers, Epidermal electronics, Science 333 (2011) 838–843.